https://doi.org/10.22226/2410-3535-2022-3-231-236

Synthesis of Tb_2O_3 nanoparticles by laser ablation in Ar gas flow

R. N. Maksimov[†,1,2], V. V. Platonov[1], A. S. Yurovskikh[2], V. A. Shitov[1], V. V. Osipov[1]

[†]romanmaksimov@e1.ru

[1]Institute of Electrophysics UB RAS, Ekaterinburg, 620016, Russia
[2]Ural Federal University named after the first President of Russia B. N. Yeltsin, Ekaterinburg, 620002, Russia

In this paper, we report on the synthesis of terbium sesquioxide (Tb_2O_3) nanopowder by laser ablation of a solid target material in Ar gas flow using an ytterbium fiber laser with an average power of 300 W. The as-synthesized nanoparticles featured spherical morphology, an average size of 13 nm and a substantially monoclinic crystal structure, whose symmetry was converted into cubic by heat treatment at 850°C under vacuum. Pressureless densification of powder compact at 1450°C yields 95.6% of the relative density indicating excellent sinterability of the produced nanoparticles. XPS analysis was used to estimate the ratio between O and Tb concentrations as [O]/[Tb] =1.51, which is close to the Tb_2O_3 stoichiometry indicating a very low content of detrimental Tb^{4+} ions. The obtained results suggest that laser ablation in Ar gas flow is a promising technique for synthesizing Tb_2O_3 nanoparticles suitable for further fabrication of advanced magnetooptical ceramics.

Keywords: terbium sesquioxide, laser ablation, nanoparticles, polymorphic phase transformation, densification.

1. Introduction

In recent years, high Verdet constant materials based on terbium sesquioxide (Tb_2O_3) have attracted considerable interest as promising magnetoactive media for Faraday isolators used in high-power near-IR laser sources [1–3]. The intensity of research and development in this direction has risen significantly since Veber et al. demonstrated the first growth of millimeter-sized cubic Tb_2O_3 single crystals using a controlled atmosphere flux method in 2015 [4]. Shortly afterwards, it was shown that Tb_2O_3 ceramic materials provide critical advantages over their single-crystalline counterparts including larger sizes and improved optical quality [5,6].

The main difficulty in fabricating high performance Tb_2O_3 ceramics consists in achieving a pore-free microstructure of the final sintered samples at the temperature lower than the phase transition point of Tb_2O_3 from the cubic to the monoclinic structure (≈1550°C) [7–9]. Partial substitution of Tb^{3+} cations for Y^{3+} or Lu^{3+} cations in Tb_2O_3 matrix can be used to inhibit the phase conversion [5,6,10,11] but the thermal conductivity and Verdet constant of the obtained solid solutions are inferior to those of parent composition. In this regard, pressure-assisted densification methods such as hot pressing and hot isostatic pressing (HIPing) are crucial for manufacturing "pure" and fully dense Tb_2O_3 ceramics at the sintering temperatures below 1550°C.

Preparation of transparent ceramics using a capsule-free post-HIP treatment includes pressureless sintering of green bodies to a relative density level >95% for elimination of surface connected porosity. Consequently, ultrafine powders with a spherical morphology and small particle size providing a high sintering activity are important for this technology. Recently, a great attention has been paid to the synthesis of terbium oxide nanocrystalline powders using wet chemical techniques such as the self-propagating high-temperature synthesis (SHS) and the thermal decomposition of various precursors [9,12–14]. However, the as-synthesized powders consist of large aggregates and typically exhibit a sponge-like porous morphology suggesting its insufficient densification at relatively low temperatures.

One of the alternative physical methods for producing oxide nano-sized particles is laser ablation, which consists in evaporating a solid target material using a high-power laser, with the eventual condensation of the vapor carried out in a buffer gas flow. The laser ablation synthesis of loosely agglomerated nanopowders based on ZrO_2 and Y_2O_3 with an average particle size 10–20 nm using radiation of CO_2 or Yb fiber lasers has been intensively studied [15,16]. Indeed, the properties of the as-obtained nanoparticles are strongly dependent on the pressure and composition of the buffer gas used to control the oxidation state of metal ions in certain oxides. For instance, nano-sized particles with a chemical composition close to Fe_3O_4 were synthesized by CO_2-laser ablation of an Fe_2O_3 target in Ar gas flow [17]. With respect to terbium oxide, this feature of the method can be used for reducing the relative content of tetravalent terbium in nanopowders, which adversely affects the magneto-optical characteristics of the final sintered Tb_2O_3 ceramics.

Thus, the aim of the present work is to synthesize and characterize terbium oxide nanoparticles by laser ablation in an Ar gas flow using a high-power Yb fiber laser.

2. Materials and methods

In order to synthesize terbium oxide nanoparticles in Ar gas flow, we updated the original experimental setup based on an LS-07N ytterbium fiber laser (Fig. 1, (1)), which was previously described in [16]. The laser radiation was focused at the surface of a solid target (4) placed inside the evaporation chamber (3) into a spot of 430 μm diameter

using an optical head (2) having a focal length of 400 mm. The target of 65 mm diameter, prepared by uniaxial pressing and sintering of terbium oxide powder (4N, Lanhit Company, Russia), was rotated and simultaneously moved in the radial direction during the ablation process to provide homogeneous wear of the surface. The natural flow of inert gas medium inside the laser setup was provided through the bag filter (9) from the vessel (5) containing high purity Ar gas (99.993 vol.%, Industrial Gases Russia) at the volume rate of 5 m^3/h controlled by needle valve (6). The volumetric rate and pressure of the gas flow were measured using variable area flow meter (7) and pressure gage (8), respectively. Nano- and micron-sized particles (melt droplets and fragments of target) along with gas flow were initially transferred to cyclones (10) where almost all coarse fractions (>10 μm) were deposited. The majority of nano-sized particles were collected in the following bag filter (11). Then the buffer gas was cleaned of aerosol in the next filter (12) before being released into the atmosphere.

The morphology of the as-synthesized terbium oxide nanoparticles was investigated using a JEOL JEM 2100 (JEOL Ltd., Japan) transmission electron microscope (TEM). The obtained TEM images were processed with the ImageJ software and an area equivalent diameter of at least 800 particles was measured to evaluate the particle size distribution. The specific surface area of the obtained nanopowder was measured according to the Brunauer-Emmett-Teller (BET) method with a TriStar 3000 gas adsorption analyzer (Micromeritics, USA). The crystal structure and phase evolution of the nanopowder were studied during heating up to 1150°C under vacuum by means of non-ambient X-Ray diffraction using a D8 Advance diffractometer (Bruker AXS, Germany) with an Anton-Paar HTK 1200N high temperature chamber in the 25° – 50° 2θ range in Cu K_α radiation. The sintering behavior of the as-synthesized nanoparticles was investigated during heating up to 1450°C with a heating rate of 3°C/min under a vacuum of 0.4 Pa using a DIL 402 C horizontal dilatometer (NETZSCH, Germany). For the dilatometry test, around 600 mg of nanopowder were uniaxially dry pressed at 50 MPa into cylindrical compact of 8 mm diameter and 5.5 mm height. In order to determine the ratio between O and Tb concentrations ([O]/[Tb]) in the as-synthesized nanoparticles, the X-ray photoelectron spectrum was recorded using a K-Alpha+ spectrometer (Thermo Fisher Scientific, USA) equipped with a hemispherical energy analyzer and an Al K_α X-ray source (hν=1456.6 eV). The spectrometer was calibrated using the binding energies of gold (Au $4f_{7/2}$, 83.95 eV), silver (Ag $3d_{5/2}$, 368.3 eV) and copper (Cu $2p_{3/2}$, 932.6 eV).

3. Results and Discussion

During the synthesis of nanopowder, the laser generated rectangular pulses of 120 μs duration at 1070 nm with a duty factor of 2 and at a peak power of 600 W. As with the synthesis of Nd: Y_2O_3 nanoparticles [16], no massive spattering of large (>10 μm) melt droplets was observed under these conditions; therefore, the evaporation regime was deemed to be optimal. The production rate was estimated to be 24 g/h. The volume rate of gas flow was chosen to be 5 m^3/h for ensuring an aerosol flow rate, at which coarse fragments of target and melt droplets were effectively deposited in the cyclones. According to our experiments, the average particle size remained practically unchanged using the gas flow rate in the range 1–6 m^3/h. In addition, a decrease in the volume rate of gas flow down to 1 m^3/h leads to a decrease in the amount of nanopowder collected in the bag filter due to an increase in the portion of nanoparticles deposited in the evaporation chamber.

According to the TEM observations, the as-synthesized nanoparticles exhibiting an almost spherical shape are assembled into loosely bound aggregates (Fig. 2 a). The size distribution of nanoparticles is lognormal (Fig. 2 b), with the average particle size reaching 13 nm. From the BET analysis, the specific surface area of the obtained nanopowder was determined as 59 m^2/g. A low degree of agglomeration and high surface energy of laser-ablated nanoparticles comprise suitable properties for uniform packing and densification of powder compact to the desired density at temperatures below the phase transition point of terbium oxide.

The results of XRD analysis (Table 1) revealed that the raw terbium oxide powder used for the preparation of the laser target comprises triclinic $Tb_{11}O_{20}$ (ICSD PDF No. 03-065-4511) and cubic $TbO_{1.81}$ (ICSD PDF No. 01-075-0275) phases. Since the triclinic structure is formed only for higher terbium oxides ($TbO_{1.72-1.82}$) [18–20], it can be concluded that the chemical composition of the initial target is close

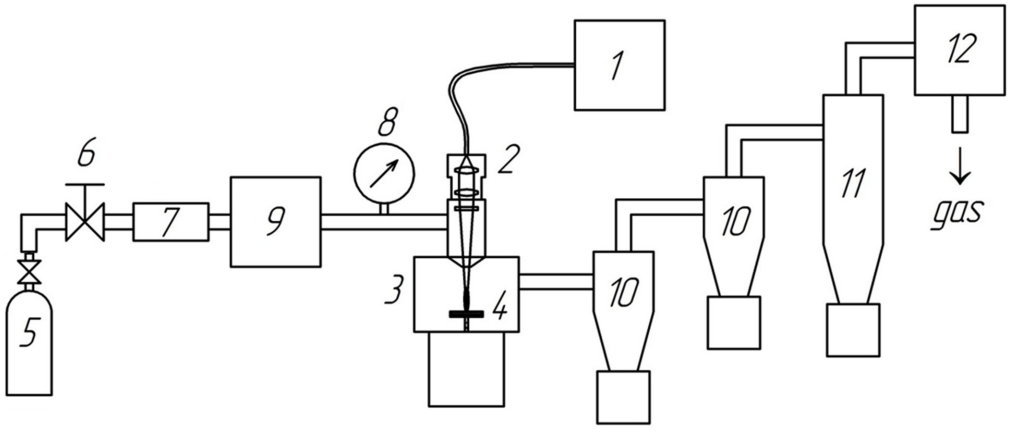

Fig. 1. Block-scheme of experimental setup developed for laser ablation synthesis of terbium oxide nanoparticles in Ar gas flow.

to $TbO_{1.82}$. Regarding the as-obtained nanoparticles, the diffraction pattern registered at room temperature can be indexed to a mixture of two Tb_2O_3 phases: (1) the monoclinic B-modification (ICSD PDF No. 01-074-2131) and (2) the cubic C-modification (ICSD PDF No. 00-021-1208). The size of the coherent scattering region was estimated to be 12 nm, which is in good agreement with TEM observations indicating a low degree of nanoparticle agglomeration.

Zhang et al. showed that the calcination and sintering processes of Tb_2O_3 nanopowders should be carried out in an oxygen-free atmosphere to avoid formation of $TbO_{1.81}$ phase during cooling down [8]. Figure 3 shows changes in the X-ray diffraction patterns of the produced terbium oxide nanoparticles during heating up to 1150°C under vacuum. The intensity of the observed (2 2 2), (0 0 4) and (4 1 1) diffraction peaks specific to the cubic phase starts to

Table 1. XRD data for solid target and as-obtained nanopowder.

	Phase composition	Content, wt.%	Lattice parameters
Solid target	$Tb_{11}O_{20}$, triclinic P-1	86	a=14.056 Å, b=3.552 Å, c=8.722 Å, α=90.02°, β=99.97°, γ=95.88°
	$TbO_{1.81}$, cubic Fm-3m	14	a=5.297 Å
Nanopowder	Tb_2O_3, monoclinic C2/m	98.5	a=14.056 Å, b=3.552 Å, c=8.722 Å, β=100.3°
	Tb_2O_3, cubic Ia-3	1.5	a=10.737 Å

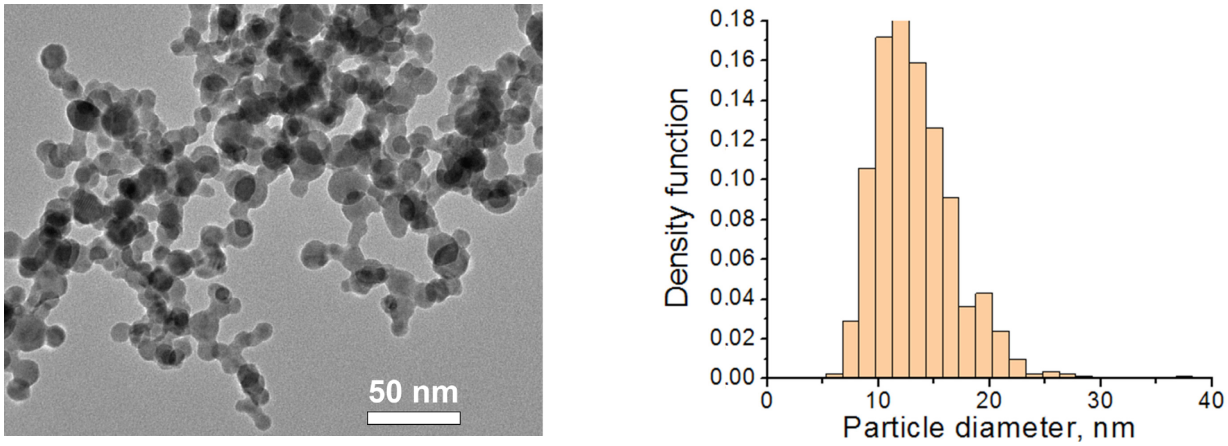

a b

Fig. 2. TEM image of the as-synthesized terbium oxide nanopowder (a) and particle size distribution histogram (b).

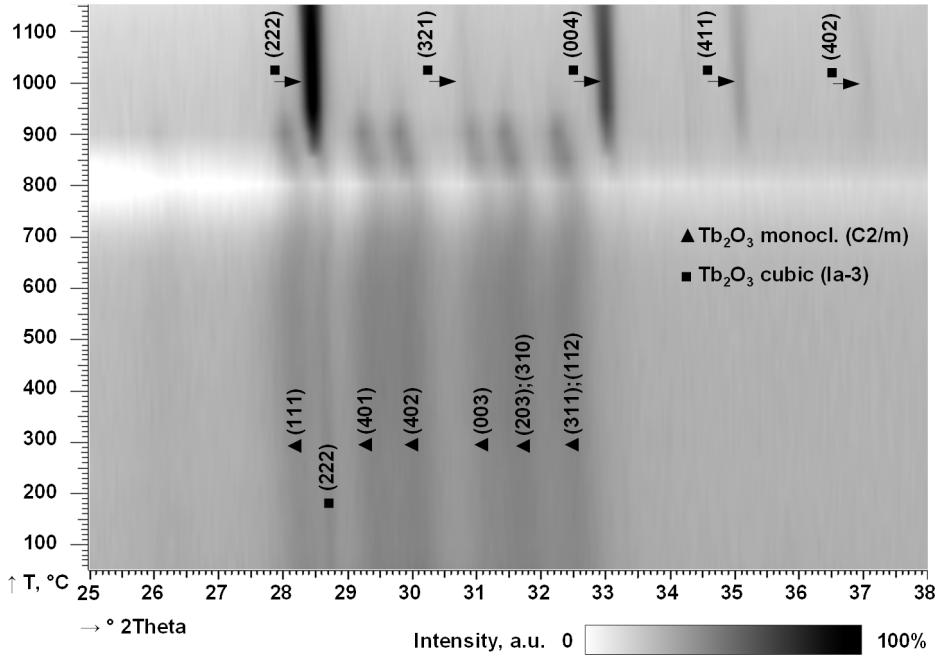

Fig. 3. X-ray diffractogram showing the phase evolution of Tb_2O_3 nanopowder during heating up from 50°C to 1150°C.

gradually increase from 850°C indicating the beginning of B→C phase transition; above 950°C, the nanoparticles are fully transformed to the cubic phase. Background and line position fluctuations in the temperature range 750–850°C are attributed to a rapid powder agglomeration causing a shift of the sample surface from the acquisition surface.

Tb_2O_3 is known to exist in the cubic Ia-3 space group (bixbyite-type) and the reversible C→B phase transition was found above 1500°C [7–9]. In addition, the phase transition to the monoclinic C2/m phase was observed under 0.6 GPa at 1000°C [21]. The crystallization of terbium sesquioxide in the metastable state during gas-phase synthesis can be explained by the Gibbs-Thomson effect [22]. The pressure difference Δp across the curved surface of a spherical particle of radius r is related to the surface tension γ: $\Delta p = 2\gamma / r$. If we assume that $r = 6.5$ nm and $\gamma = 0.79$ N/m at 1000°C [23], then $\Delta p = 0.243$ GPa, which is the reasonable order of magnitude for the pressure induced phase conversion in the process of laser synthesis. The value of the surface tension can be even higher in nano-sized particles than the value for a flat surface which would further increase the pressure.

The temperature dependences of shrinkage and shrinkage rate of Tb_2O_3 powder compact are presented in Fig. 4a. The sample shows a minor shrinkage in the temperature range 200–600°C attributed to a low temperature sintering and neck formation. Rapid densification of powder compact starts at around 650°C and the shrinkage rate reaches a maximum value of $-2.47 \cdot 10^{-3}$ min^{-1} at 709°C. At the maximum shrinkage rate, the linear shrinkage is −15.9% corresponding to the relative density of 36.9% with respect to the theoretical density of B-Tb_2O_3 (8.56 g/cm³). After 800°C a slight retardation in shrinkage is observed due to the B→C phase conversion of Tb_2O_3 accompanied by an increase in the volume of unit cell. The shrinkage value in the temperature range 800–1000°C is as low as −4.3% because of the competing processes of the transformation induced expansion and natural temperature shrinkage. The sample continues to densify until the final sintering temperature of 1450°C, at which the shrinkage reaches −37% corresponding to 95.6% of density relative to theoretical value of C-Tb_2O_3 (7.82 g/cm³). After sintering and cooling down under vacuum the sample preserved the cubic bixbyite-type crystal structure with the lattice constant $a = 10.729$ Å and no secondary phases were identified by XRD analysis (Fig. 4b). It appears that Tb_2O_3 nanoparticles obtained by laser ablation have higher sintering activity compared with nanopowder of similar composition produced by the SHS method, for which only 82% of the relative density can be attained by pressureless sintering at 1450°C [24].

An XPS study was conducted in order to evaluate the atomic ratio O/Tb in the as-synthesized nanoparticles. The survey scan in Fig. 5a demonstrates the signals corresponding to electrons photoemitted by Tb (4d, $3d_{5/2}$, $3d_{3/2}$), C (1s) and O (1s) as well as the Auger line of oxygen. The C 1s photoelectron peak corresponds to the accidental carbon impurities present at the surface. The area under the Tb $3d_{5/2}$ and O 1s peaks was calculated to determine the relative content of terbium and oxygen (inset of Fig. 5a). The high resolution O 1s spectrum in the range of 526–535 eV (Fig. 5b) displays a broad band, which was fitted into two overlapped peaks with binding energies of 529.1 and 531.7 eV. The first peak is related to the lattice oxygen while the second is attributed to the oxygen species such as carbonates, water and OH^- groups adsorbed onto the surface of the nanopowders [25,26]. Considering that the peak at 529.1 eV is the only peak of oxygen characterizing the Tb-O bond [27], we estimated the ratio [O]/[Tb] as ≈1.51, which is very close to the stoichiometric ratio in Tb_2O_3.

It is known that Tb^{4+} absorption centers cause a thermal lens effect during laser operation [6,28]. This problem is probably due to the presence in the raw oxide of terbium in the +3 and +4 oxidation states. Typically, the reduction of commercially available terbium oxide (labeled as Tb_4O_7) powder to $TbO_{1.5}$ stoichiometry is carried out by calcining at 1250°C or 1300°C under an inert or reducing gas flow [4,6]. However, subsequent ball milling usually required to crush hard agglomerates formed after the calcination step causes undesirable contamination of the powder by the milling media. In addition, a certain amount of Tb^{4+}, which is detrimental for magnetooptical properties, can still be detected in the sintered ceramics and calcined powder [6,29]. The process of obtaining a terbium oxide nanopowder having

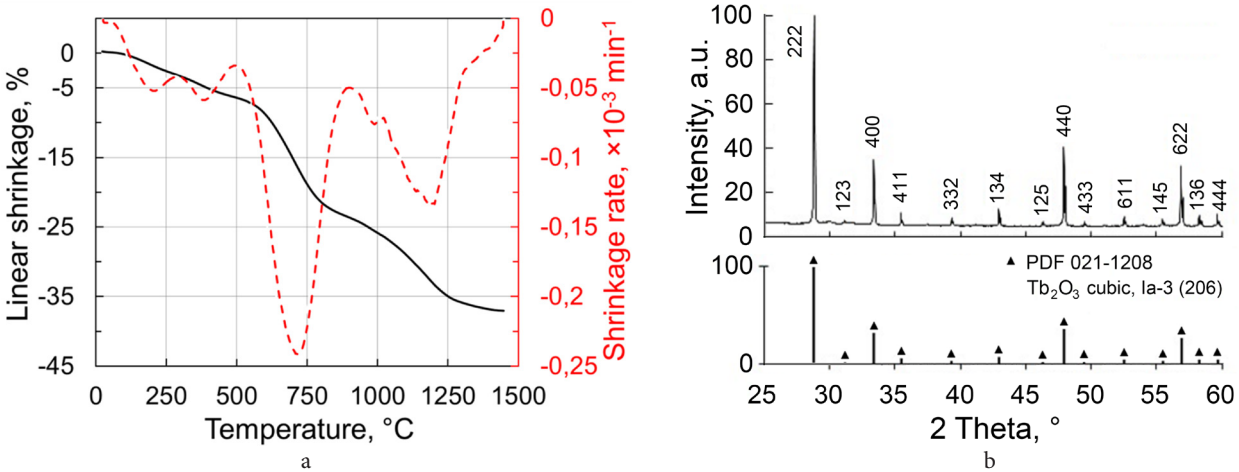

a b

Fig. 4. (Color online) Linear shrinkage and shrinkage rate of Tb_2O_3 nanopowder compact during heating up to 1450°C under vacuum (a) and X-ray diffractogram of the sample after sintering (b).

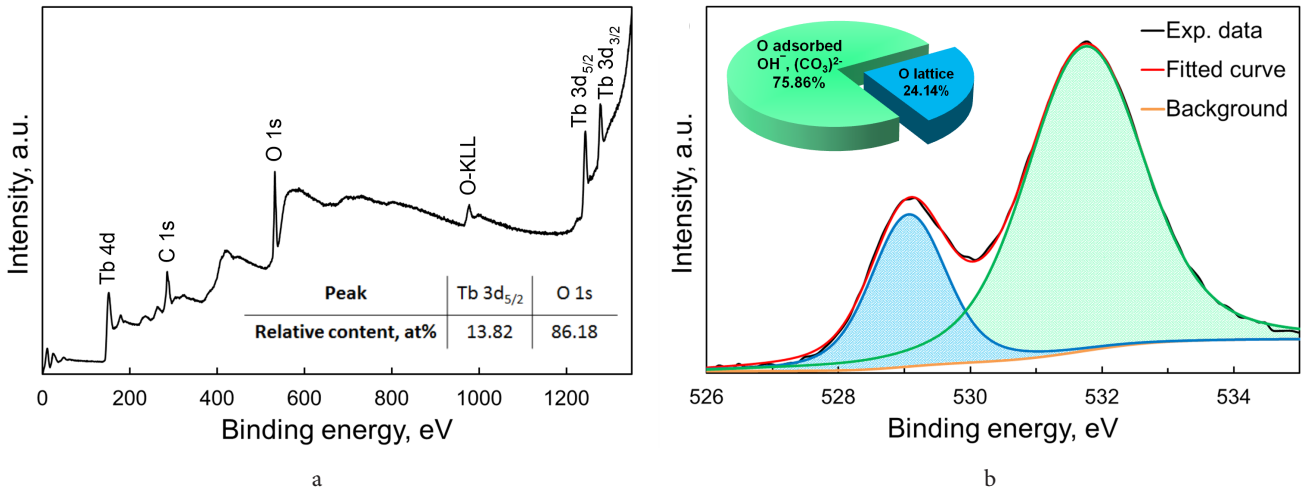

Fig. 5. (Color online) Survey XPS scan of Tb_2O_3 nanopowder (a) and XPS spectrum of O 1s (b).

a lower degree of oxidation $TbO_{1.51}$ during the evaporation of the solid target with the estimated chemical composition $TbO_{1.82}$ can be explained as follows. The initial $TbO_{1.82}$ is reduced almost to $TbO_{1.5}$ under heating by laser radiation to the melting temperature (2410°C) followed by evaporation of the obtained sesquioxide. On the other hand, since the formation of nanoparticles in a laser plume occurs very fast (during ≈1 ms), there is no time for their oxidation. Therefore the melted layer on the target surface also does not have time to be oxidized following the end of exposure to laser radiation and the already partially reduced terbium oxide undergoes further evaporation.

Conclusions

The elaboration of an efficient process for synthesizing ultrafine and stoichiometric Tb_2O_3 powders with excellent sinterability is a highly relevant task for ceramic technology because tetravalent terbium cations cause adverse effect on magnetooptical performance. In this work, spherical terbium oxide nanoparticles having an average size of 13 nm were synthesized by laser ablation in an argon flow using an ytterbium fiber laser generating repetitively pulsed radiation with an average power of 300 W. Due to the short time for the formation of nanoparticles in the laser plume and fast cooling of the melt at the target surface and utilization of Ar gas, it was possible to obtain terbium oxide nanopowder having a chemical composition very close to $TbO_{1.5}$ by evaporating the higher oxide $TbO_{1.82}$. The synthesized nanoparticles possess a mainly monoclinic crystal structure, which can be modified into a cubic structure following calcination at 850°C under vacuum. The laser-ablated nanoparticles could be promising for the fabrication of advanced magnetooptical Tb_2O_3 ceramics owing to their high sintering activity and extremely high content of active Tb^{3+} ions. The developed approach is valuable in producing other compounds where control of oxygen content is an important factor.

Acknowledgements. The reported study was carried out with the use of grant №22-23-00658 of the Russian Science Foundation, https://rscf.ru/en/project/22-23-00658/

References

1. K. J. Carothers, R. A. Norwood, J. Pyun. Chem. Mater. 34, 2531 (2022). Crossref
2. D. Vojna, O. Slezak, A. Lucianetti, T. Mocek. Appl. Sci. 9, 3160 (2019). Crossref
3. J. Dai, J. Li. Scr. Mater. 155, 78 (2018). Crossref
4. P. Veber, M. Velazquez, G. Gadret, D. Rytz, M. Peltzc, R. Decourta. CrystEngComm. 3, 492 (2015). Crossref
5. A. Ikesue, Y. L. Aung, S. Makikawa, A. Yahagi. Opt. Lett. 42, 4399 (2017). Crossref
6. A. Ikesue, Y. L. Aung, S. Makikawa, A. Yahagi. Materials. 12, 421 (2019). Crossref
7. M. Zinkevich. Prog. Mater. Sci. 52, 597 (2007). Crossref
8. J. Zhang, H. Chen, J. Wang, D. Wang, D. Han, J. Zhang, S. Wang. Scr. Mater. 171, 108 (2019). Crossref
9. S. S. Balabanov, D. A. Permin, E. Ye. Rostokina, S. V. Egorov, A. A. Sorokin, D. D. Kuznetsov. Ceram. Int. 43, 16569 (2017). Crossref
10. J. Zhang, H. Chen, J. Wang, D. Wang, D. Han, J. Zhang, S. Wang. J. Eur. Ceram. Soc. 41, 2818 (2021). Crossref
11. M. Yang, D. Zhou, J. Xu, T. Tian, R. Jia, Z. Wang. J. Eur. Ceram. Soc. 39, 5005 (2019). Crossref
12. B. M. Abu-Zied, A.-R. N. Mohamed, A. M. Asiri. J. Nanosci. Nanotechnol. 15, 4487 (2015). Crossref
13. P. V. Fursikov, M. N. Abdusalyamova, F. A. Makhmudov, E. N. Shairmardanov, I. D. Kovalev, D. Yu. Kovalev, R. B. Morgunov, O. V. Koplak, A. A. Volodin, I. I. Khodos, Y. M. Shulga. J. Alloys Compd. 657, 163 (2016). Crossref
14. F. Kai, L. Bin, C. Hongmei, W. Shaofan, W. Yan, L. Yongxing. J. Synth. Cryst. 50, 80 (2021).
15. H. D. Kurland, J. Grabow, Chr. Stotzel, F. A. Muller. J. Ceram. Sci. Technol. 5, 275 (2014). Crossref
16. V. V. Osipov, V. V. Platonov, V. V. Lisenkov, E. V. Tikhonov, A. V. Podkin. Appl. Phys. A. 124, 3 (2018). Crossref
17. V. V. Osipov, V. V. Platonov, M. A. Uimin, A. V. Podkin. Tech. Phys. 57, 543 (2012). Crossref
18. V. B. Glushkova. Polymorphism of Oxides of the Rare-Earth Elements. Leningrad, Nauka (1967) 133 p. (in Russian)
19. S. Baran, R. Duraj, A. Hoser, B. Penc, A. Szytula. Acta Phys. Pol. A. 123, 98 (2013). Crossref

20. R. T. Tuenge, L. Eyring. J. Solid State Chem. 41, 75 (1982). Crossref
21. H. R. Hoekstra. Inorg. Chem. 5, 754 (1966). Crossref
22. D. A. Porter, K. E. Easterling, M. Y. Sherif. Phase transformation in metals and alloys. 3rd edn. Boca Raton, CRC Press (2009) 521 p.
23. T. Ishikawa, C. Koyama, H. Oda, H. Saruwatari, P.-F. Paradis. Int. J. Microgravity Sci. Appl. 39, 390101 (2022). Crossref
24. S. S. Balabanov, D. A. Permin, E. Ye. Rostokina, S. V. Egorov, A. A. Sorokin. J. Adv. Ceram. 7, 362 (2018). Crossref
25. F. Mercier, C. Alliot, L. Bion, N. Thromat, P. Toulhoat. J. Electron Spectrosc. Relat. Phenom. 150, 21 (2006). Crossref
26. S. V. Belaya, V. V. Bakovets, I. P. Asanov, I. V. Korolkov, V. S. Sulyaeva. Chem. Vap. Depos. 21, 150 (2015). Crossref
27. Handbook of X-ray Photoelectron Spectroscopy (ed. by J. F. Moulder, W. F. Stickle, P. E. Sobol, K. D. Bomben). Minnesora, Eden Prairie (1992) 261 p.
28. I. Snetkov, A. Starobor, O. Palashov, S. Balabanov, D. Permin, E. Rostokina. Opt. Mater. 120, 111466 (2021). Crossref
29. M. Velazquez, S. Pechev, M. Duttine, A. Wattiaux, C. Labrugere, Ph. Veber, S. Buffiere, D. Denux. J. Solid State Chem. 264, 91 (2018). Crossref